J. Lindberg, T. Setälä, M. Kaivola, and A. T. Friberg, Spatial coherence effects in light scattering from metallic nanocylinders, Journal of the Optical Society of America A 23, 1349-1358 (2006).

Spatial coherence effects in light scattering from metallic nanocylinders

Jari Lindberg, Tero Setälä, and Matti Kaivola

Department of Engineering Physics and Mathematics, Helsinki University of Technology, P.O. Box 3500, FI-02015 TKK, Finland

Ari T. Friberg

Royal Institute of Technology, Department of Microelectronics and Information Technology, Electrum 229, SE-164 40 Kista, Sweden

Received September 30, 2005; accepted October 28, 2005; posted December 1, 2005 (Doc. ID 65065)

We study the scattering of a partially coherent electromagnetic beam from metallic nanocylinders and analyze the effects of plasmon resonances on the coherence and polarization properties of the optical near field. We employ the coherent-mode representation for the incident field and solve the scattering problem independently for each mode by using a boundary-integral method. Our results show that the plasmon resonances may significantly affect the coherence and polarization characteristics of the near field and that partial coherence influences the energy flow in nanocylinder arrays. © 2006 Optical Society of America

OCIS codes: 030.1640, 030.4070, 290.5850.

1. INTRODUCTION

Surface plasmon and phonon polaritons are known to play a central role in the properties of optical near fields. Often the analysis of plasmon effects is restricted to deterministic (monochromatic) optical fields, but some studies also involving the fluctuating character of light have appeared. For example, it has been shown that due to absorption the coherence length in the near field can be much smaller than the wavelength or that it can extend over several tens of wavelengths, even for thermal sources, due to surface polariton excitations.[1,2] Also, the excitations can cause the near-field spectrum to differ significantly from the corresponding source and far-field spectra.[3] Furthermore, a study for assessing the effects of surface polaritons on the degree of polarization in the near field has also been reported.[4] These recent discoveries indicate that when the coherence theory is applied to nanoscale electromagnetic fields, novel effects can be expected.

Besides surface plasmons on a planar surface, localized plasmon resonances can be excited in metallic nanoparticles or nanowires. Such an excitation can lead to a large scattering cross section and to a strong enhancement of the electromagnetic field around the particle at the resonant wavelength.[5–9] Currently there is considerable interest in studies of nanoparticle chains[10–14] and nanowires,[5,15–17] as these systems can act as near-field waveguides enabling light guiding at subwavelength scales.

In this work we investigate the scattering of a TM-polarized one-dimensional (1D) Gaussian Schell-model (GSM) beam from a system consisting of one or more metallic nanowires with cylindrical cross section. We analyze the changes caused by plasmon resonances on the (spatial) coherence and polarization properties of the optical near field around the scatterer. We characterize the coherence in the optical near field in terms of the electromagnetic degree of coherence[18,19] and the three-dimensional (3D) degree of polarization.[4,20] The scattering problem is treated by employing the theory of coherent modes[21,22] and solving the scattered modes with a boundary-integral method.[8,23–26]

The paper is organized as follows. In Section 2 the cross-spectral density tensors and the quantities for the description of partial coherence and partial polarization in electromagnetic fields are introduced. In Section 3 we show how the coherence tensors can be determined by making use of the coherent modes and the angular-spectrum representation of the wave fields. In Section 4 we apply the concepts of Section 3 to a TM-polarized 1D GSM beam. The boundary-integral method is described in Section 5, and the results are presented and discussed in Section 6. The work is summarized in Section 7.

2. CROSS-SPECTRAL DENSITY TENSORS

The geometries that we consider are invariant in the z direction and, therefore, can be treated as two dimensional (2D). In such a system each realization of the fluctuating electromagnetic field can be represented as a superposition of transverse electric (TE) and transverse magnetic (TM) field components. The TE-polarized and TM-polarized waves are determined by, respectively, a single electric field and a single magnetic field component, which, in this case, point in the z direction.

The coherence properties of a partially coherent, statistically stationary (in the wide sense) electromagnetic field are, at angular frequency ω, characterized by the electric, magnetic, and two mixed cross-spectral density tensors, whose components are, respectively, given by[21]

$$W_{kl}^{(e)}(\mathbf{r}_1,\mathbf{r}_2,\omega)=\langle E_k^*(\mathbf{r}_1,\omega)E_l(\mathbf{r}_2,\omega)\rangle, \quad (1)$$

$$W_{kl}^{(h)}(\mathbf{r}_1,\mathbf{r}_2,\omega)=\langle H_k^*(\mathbf{r}_1,\omega)H_l(\mathbf{r}_2,\omega)\rangle, \quad (2)$$

$$W_{kl}^{(m)}(\mathbf{r}_1,\mathbf{r}_2,\omega)=\langle E_k^*(\mathbf{r}_1,\omega)H_l(\mathbf{r}_2,\omega)\rangle, \quad (3)$$

$$W_{kl}^{(n)}(\mathbf{r}_1,\mathbf{r}_2,\omega)=\langle H_k^*(\mathbf{r}_1,\omega)E_l(\mathbf{r}_2,\omega)\rangle. \quad (4)$$

The quantities $E_{l,k}$ and $H_{l,k}$, with $(l,k)=(x,y,z)$, denote the Cartesian components of, respectively, the electric and magnetic field in the electromagnetic field realization. Furthermore, $\mathbf{r}_i=(x_i,y_i)$, with $i=(1,2)$, refers to two points in space, the asterisk denotes complex conjugation, and the angle brackets stand for ensemble averaging.

We will now limit our analysis to the TM-polarized light, since the plasmon resonances in a 2D geometry can occur only for light with this polarization direction. For the TM-polarized light the magnetic cross-spectral density tensor has only one nonzero element, namely, $W_{zz}^{(h)}$. Since

$$\mathbf{E}(\mathbf{r},\omega)=-\frac{1}{i\omega\epsilon(\mathbf{r},\omega)}\nabla\times\mathbf{H}(\mathbf{r},\omega), \quad (5)$$

the magnetic field component H_z determines the components E_x and E_y of the electric field realization. This implies that the elements of the electric cross-spectral density tensor for the TM-polarized light are given by

$$W_{xx}^{(e)}(\mathbf{r}_1,\mathbf{r}_2,\omega)=\frac{1}{\omega^2\epsilon^*(\mathbf{r}_1,\omega)\epsilon(\mathbf{r}_2,\omega)}\frac{\partial^2 W_{zz}^{(h)}(\mathbf{r}_1,\mathbf{r}_2,\omega)}{\partial y_1\partial y_2}, \quad (6)$$

$$W_{xy}^{(e)}(\mathbf{r}_1,\mathbf{r}_2,\omega)=-\frac{1}{\omega^2\epsilon^*(\mathbf{r}_1,\omega)\epsilon(\mathbf{r}_2,\omega)}\frac{\partial^2 W_{zz}^{(h)}(\mathbf{r}_1,\mathbf{r}_2,\omega)}{\partial y_1\partial x_2}, \quad (7)$$

$$W_{yx}^{(e)}(\mathbf{r}_1,\mathbf{r}_2,\omega)=-\frac{1}{\omega^2\epsilon^*(\mathbf{r}_1,\omega)\epsilon(\mathbf{r}_2,\omega)}\frac{\partial^2 W_{zz}^{(h)}(\mathbf{r}_1,\mathbf{r}_2,\omega)}{\partial x_1\partial y_2}, \quad (8)$$

$$W_{yy}^{(e)}(\mathbf{r}_1,\mathbf{r}_2,\omega)=\frac{1}{\omega^2\epsilon^*(\mathbf{r}_1,\omega)\epsilon(\mathbf{r}_2,\omega)}\frac{\partial^2 W_{zz}^{(h)}(\mathbf{r}_1,\mathbf{r}_2,\omega)}{\partial x_1\partial x_2}, \quad (9)$$

while all the other elements are zero. The permittivity (in general, complex) is given by $\epsilon(\mathbf{r},\omega)=\epsilon_0\epsilon_r(\mathbf{r},\omega)$, with ϵ_0 and $\epsilon_r(\mathbf{r},\omega)$ denoting the dielectric constant of vacuum and the relative permittivity of the medium, respectively. Furthermore, for later purposes, we note that the components of the averaged Poynting vector $\langle\mathcal{S}(\mathbf{r})\rangle$ are given by[22]

$$\langle\mathcal{S}_k(\mathbf{r})\rangle=\frac{1}{4}\sum_{lm}\epsilon_{klm}[W_{lm}^{(m)}(\mathbf{r},\mathbf{r},\omega)-W_{lm}^{(n)}(\mathbf{r},\mathbf{r},\omega)], \quad (10)$$

where ϵ_{klm} is the Levi–Cività antisymmetric unit tensor.

To describe the (spatial) coherence properties of random electromagnetic fields, we employ the electromagnetic degree of coherence and the 3D degree of polarization. The electromagnetic degree of coherence $\mu_{el}(\mathbf{r}_1,\mathbf{r}_2,\omega)$ is defined as[18]

$$\mu_{el}(\mathbf{r}_1,\mathbf{r}_2,\omega)=\frac{\|\mathbf{W}^{(e)}(\mathbf{r}_1,\mathbf{r}_2,\omega)\|_F}{[S(\mathbf{r}_1,\omega)S(\mathbf{r}_2,\omega)]^{1/2}}, \quad (11)$$

where $\mathbf{W}^{(e)}(\mathbf{r}_1,\mathbf{r}_2,\omega)$ is the 3D electric cross-spectral density tensor, $\|\mathbf{A}\|_F\equiv[\mathrm{tr}(\mathbf{A}\cdot\mathbf{A}^\dagger)]^{1/2}$ is the Frobenius norm, where tr and † denote trace and Hermitian adjoint, respectively, and $S(\mathbf{r},\omega)=\mathrm{tr}[\mathbf{W}^{(e)}(\mathbf{r},\mathbf{r},\omega)]$ is the spectral density at angular frequency ω. The 3D degree of polarization $P_3(\mathbf{r},\omega)$ is given by[4,20]

$$P_3^2(\mathbf{r},\omega)=\frac{3}{2}\left\{\frac{\mathrm{tr}\{[\mathbf{W}^{(e)}(\mathbf{r},\mathbf{r},\omega)]^2\}}{\mathrm{tr}[\mathbf{W}^{(e)}(\mathbf{r},\mathbf{r},\omega)]}-\frac{1}{3}\right\}. \quad (12)$$

Physically $\mu_{el}(\mathbf{r}_1,\mathbf{r}_2,\omega)$ and $P_3(\mathbf{r},\omega)$ characterize the correlations of orthogonal electric field components at two points and at one point, respectively.

3. COHERENT-MODE REPRESENTATION

Across the plane $y=0$ the coherent-mode representation of the magnetic cross-spectral density tensor of the incident field is of the form

$$W_{zz}^{(h),\mathrm{inc}}(x_1,0,x_2,0,\omega)=\sum_{q=0}^{\infty}\lambda_q(\omega)\phi_q^*(x_1,0,\omega)\phi_q(x_2,0,\omega), \quad (13)$$

where $\lambda_q(\omega)$ are the eigenvalues and $\phi_q(x,0,\omega)$ are the orthonormal eigenfunctions of the homogeneous Fredholm integral equation

$$\int_{-\infty}^{\infty}W_{zz}^{(h),\mathrm{inc}}(x_1,0,x_2,0,\omega)\phi_q(x_1,0,\omega)\mathrm{d}x_1=\lambda_q(\omega)\phi_q(x_2,0,\omega). \quad (14)$$

The modes $\phi_q(x,y,\omega)$ are mutually uncorrelated and thus propagate without interference. The propagation of the modes is governed by the 2D Helmholtz equation

$$\nabla^2\phi_q(x,y,\omega)+k_0^2n^2\phi_q(x,y,\omega)=0, \quad (15)$$

where k_0 is the free-space wave number and n is the refractive index of the medium. Furthermore, as each field realization obeys the Sommerfeld radiation condition and the boundary conditions at the interfaces, the same must be true for the modes $\phi_q(x,y,\omega)$.

We assume that the field propagates into the region $y<0$. When the mode $\phi_q(x,y,\omega)$ is known across the transverse plane $y=0$, the mode within the region $y\leqslant 0$ can be written in terms of the angular-spectrum representation, which in general may contain both propagating and evanescent components. In two dimensions the representation is of the form[22]

$$\phi_q(x,y,\omega)=\int_{-\infty}^{\infty}A_q(\alpha,\omega)\exp\{i[\alpha x-s(\alpha)y]\}\mathrm{d}\alpha, \quad (16)$$

where

$$A_q(\alpha,\omega)=\frac{1}{2\pi}\int_{-\infty}^{\infty}\phi_q(x,0,\omega)\exp(-i\alpha x)\mathrm{d}x \tag{17}$$

is the angular spectrum and

$$s(\alpha)=\begin{cases}[(k_0n)^2-\alpha^2]^{1/2}, & |\alpha|\leqslant k_0n\\ i[\alpha^2-(k_0n)^2]^{1/2}, & \text{otherwise}\end{cases}. \tag{18}$$

Thus the magnetic cross-spectral density tensor of the incident field in the half-space $y\leqslant 0$ can be written as

$$W_{zz}^{(h),\mathrm{inc}}(x_1,y_1,x_2,y_2,\omega)=\sum_{q=0}^{\infty}\lambda_q(\omega)\phi_q^*(x_1,y_1,\omega)\phi_q(x_2,y_2,\omega). \tag{19}$$

Once the modes of the incident field are known, we can treat the scattering of the field by solving the problem independently for each mode.[22]

4. GAUSSIAN SCHELL-MODEL FIELD

In this work we consider TM-polarized optical beams whose magnetic cross-spectral density tensor component $W_{zz}^{(h)}$ at the waist plane ($y=0$) is of the Gaussian Schell-model (GSM) form. This is explicitly written as

$$\mathcal{W}_{zz}^{(h)}(x_1,0,x_2,0,\omega)=W_0\exp\left[-\frac{x_1^2+x_2^2}{4w_0^2(\omega)}\right]\exp\left[-\frac{(x_1-x_2)^2}{2\sigma_0^2(\omega)}\right], \tag{20}$$

where W_0 is a constant, $w_0(\omega)$ is the beam width of the magnetic energy density distribution, and $\sigma_0(\omega)$ is the transverse correlation length.

For the GSM beam the coherent modes are known in the analytical form[21]

$$\phi_q(x,0,\omega)=\left(\frac{2c}{\pi}\right)^{1/4}\frac{1}{(2^qq!)^{1/2}}H_q(x\sqrt{2c})\exp(-cx^2), \tag{21}$$

where $H_q(x)$ is the Hermite polynomial of order q,

$$a=\frac{1}{4w_0^2(\omega)},\quad b=\frac{1}{2\sigma_0^2(\omega)},\quad c=(a^2+2ab)^{1/2}, \tag{22}$$

and the corresponding eigenvalues are

$$\lambda_q(\omega)=\left(\frac{\pi}{a+b+c}\right)^{1/2}\left(\frac{b}{a+b+c}\right)^q. \tag{23}$$

The angular spectrum for the mode $\phi_q(x,y,\omega)$ is obtained by substituting Eq. (21) into Eq. (17), resulting in[22]

$$A_q(\alpha)=\frac{(-i)^q}{2\pi}\left(\frac{2\pi}{c}\right)^{1/4}\frac{1}{(2^qq!)^{1/2}}\exp\left(-\frac{\alpha^2}{4c}\right)H_q\left(\frac{\alpha}{\sqrt{2c}}\right). \tag{24}$$

By inserting the above angular spectrum into Eq. (16), neglecting the evanescent components, and approximating that the main contribution to the resulting integral arises from the region of small α, we obtain the following analytical expression for the mode:

$$\phi_q(x,y,\omega)=\frac{(-i)^q}{2(\gamma 2^qq!)^{1/2}}\left(\frac{2}{\pi c}\right)^{1/4}\exp\left(-ik_0ny-\frac{x^2}{4\gamma}\right)\times\left(1-\frac{1}{2c\gamma}\right)^{q/2}H_q\left(\frac{ix}{2(2c\gamma^2-\gamma)^{1/2}}\right), \tag{25}$$

where

$$\gamma=\frac{1}{4c}-\frac{iy}{2k_0n}. \tag{26}$$

Equations (19), (23), and (25) give us the coherent-mode representation for $\mathcal{H}_{zz}$ of the incident GSM beam throughout the space.

5. BOUNDARY-INTEGRAL METHOD

We employ the boundary-integral method to solve the scattering problem for each coherent mode of the incident field. In what follows we briefly outline the method and its numerical solution.[8,9,23–26]

For systems that are invariant in one direction, the behavior of the magnetic field modes associated with TM-polarized light is, in any homogeneous and isotropic region, governed by the 2D Helmholtz equation [Eq. (15)]. The solution of that equation in a closed region labeled by j can be expressed as a boundary integral:

$$\phi_j(\mathbf{r})=\oint_{s_j}\{G_j(\mathbf{r},\mathbf{r}')[\hat{n}\cdot\nabla'\phi_j(\mathbf{r}')]-\phi_j(\mathbf{r}')[\hat{n}\cdot\nabla'G_j(\mathbf{r},\mathbf{r}')]\}\mathrm{d}s', \tag{27}$$

where $\hat{n}$ denotes the outward unit vector normal to the curve s_j around the region. The Green function $G_j(\mathbf{r},\mathbf{r}')$, which satisfies the inhomogeneous 2D Helmholtz equation with a delta-function source term, is explicitly given by

$$G_j(\mathbf{r},\mathbf{r}')=\frac{i}{4}H_0^{(1)}(k_0n_j|\mathbf{r}-\mathbf{r}'|), \tag{28}$$

where $H_0^{(1)}(x)$ is the zero-order Hankel function of the first kind.

To obtain the boundary values, we take the limit of Eq. (27) as $\mathbf{r}$ approaches the point $\mathbf{r}_s$ on the boundary. The singularity at $\mathbf{r}_s=\mathbf{r}'$ is treated by deforming the boundary around the singular point with an arc of radius ϵ and taking the limit $\epsilon\to 0$. For a system consisting of two regions (interior and exterior of the scatterer) with smooth boundaries, we obtain

$$\frac{1}{2}\phi_1(\mathbf{r}_s)=\phi_1^{\mathrm{inc}}(\mathbf{r}_s)+\oint_s\{G_1(\mathbf{r}_s,\mathbf{r}')[\hat{n}_1\cdot\nabla'\phi_1(\mathbf{r}')]-\phi_1(\mathbf{r}')[\hat{n}_1\cdot\nabla'G_1(\mathbf{r}_s,\mathbf{r}')]\}\mathrm{d}s', \tag{29}$$

$$\frac{1}{2}\phi_2(\mathbf{r}_s)=\oint_s\{G_2(\mathbf{r}_s,\mathbf{r}')[\hat{n}_2\cdot\nabla'\phi_2(\mathbf{r}')]-\phi_2(\mathbf{r}')[\hat{n}_2\cdot\nabla'G_2(\mathbf{r}_s,\mathbf{r}')]\}\mathrm{d}s' \tag{30}$$

for the region outside ($j=1$) and inside ($j=2$) the scatterer, respectively. Here s denotes the boundary of the scatterer, and the incident mode is given by ϕ_1^{inc}.

We use the boundary-element method to obtain a numerical solution to the problem. The geometry and the fields are represented with cubic Lagrange shape functions,[26] and the integrals over each element are evaluated by using Gaussian quadratures. For each node on the boundary, we have four unknowns: the field and its normal derivative in the regions above and below the node. The boundary conditions for the field and its normal derivative are employed to express the unknown boundary values of the region inside the scatterer in terms of the corresponding boundary values in the exterior region of the scatterer. The equations for the mode ϕ_1 and its normal derivative ϕ_1' at the nodes can then be written in the form[25]

$$\begin{bmatrix} B_1 & C_1 \\ B_2 & C_2 \end{bmatrix} \begin{pmatrix} \phi_1 \\ \phi_1' \end{pmatrix} = \begin{pmatrix} \phi_1^{\text{inc}} \\ 0 \end{pmatrix}, \tag{31}$$

where C_j and B_j, with $j=(1,2)$, represent the integral operators in region j involving the Green function and its normal derivative, respectively. Since for a fixed frequency the left-hand side of Eq. (31) is independent of the properties of the incident field, the matrix elements need to be calculated only once for any given geometry, and thus all coherent modes of beams with different values of parameters $w_0(\omega)$ and $\sigma_0(\omega)$ can be evaluated efficiently.

6. RESULTS

We employ the theory of the previous sections to investigate the effects of plasmon resonances on the coherence and polarization properties of the near field when a TM-polarized GSM beam scatters from a single nanocylinder, two interacting cylinders, or a chain of cylinders. In any geometry the cylinders are of silver, for which the values of the refractive index are taken from Ref. 27. We consider the scattering of two beams with different coherence properties, one with $w_0=9.6\lambda$ and $\sigma_0=0.6\lambda$ and the other with $w_0=9.6\lambda$ and $\sigma_0=4.8\lambda$. Unless stated otherwise, the beams propagate in the negative y direction. For the number of modes retained in the coherent-mode representation, we use the criterion $\lambda_q(\omega)/\lambda_0(\omega)>10^{-4}$, which leads to 74 modes for the beam with $\sigma_0=0.6\lambda$ and 10 for $\sigma_0=4.8\lambda$.

First we analyze the scattering of the beam with $\sigma_0=0.6\lambda$ from a single silver cylinder having a radius of $r=25$ nm. Such an object is known to exhibit a plasmon resonance at the wavelength $\lambda\approx 340$ nm.[5,7,9] In Fig. 1(a) we show the spectral density $S(\mathbf{r},\omega)$ of the total field (incident plus scattered) on a $\log_{10}$ scale close to the cylinder for the resonant wavelength. It is seen that at resonance the field has a region of high intensity in front of the cylinder. The 3D degree of polarization $P_3(\mathbf{r},\omega)$ and the electromagnetic degree of coherence with respect to the origin, $\mu_{el}(\mathbf{r},0,\omega)$, are depicted in Figs. 1(b) and 1(c), respectively.[28] It is seen that the light in the region of high intensity in front of the scatterer is highly polarized and coherent. Furthermore, the field contains two sidelobes of lesser intensity that have a high degree of polarization and coherence. Figure 2 depicts the same quantities as those in Fig. 1 but for the off-resonance case $\lambda=375$ nm. There is no significant field enhancement, and, unlike in the resonant case, the highly polarized and coherent areas are now localized on the sides of the cylinder. We have also observed (although not shown here) that, in both resonance and off-resonance cases, the near field

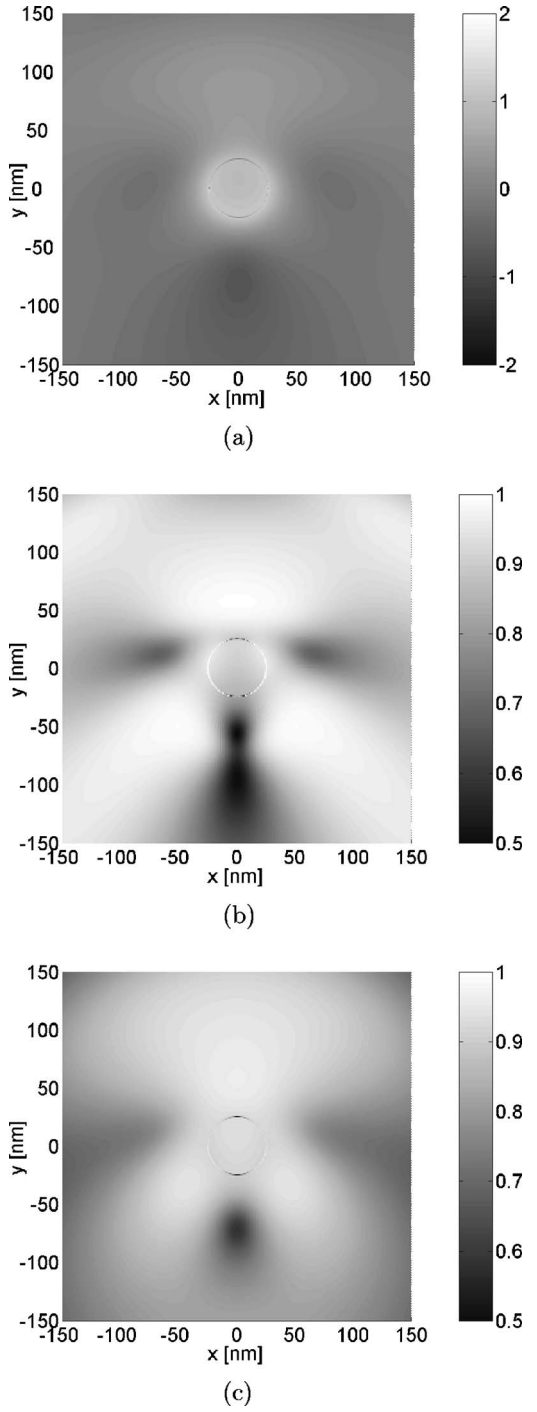

Fig. 1. Illustration of the coherence properties of the near field around a silver cylinder of radius $r=25$ nm: (a) spectral density $\log_{10}[S(\mathbf{r},\omega)]$ (arbitrary units), (b) 3D degree of polarization $P_3(\mathbf{r},\omega)$, and (c) electromagnetic degree of coherence $\mu_{el}(\mathbf{r},0,\omega)$. The incident-beam parameters are $w_0=4.8\lambda$ and $\sigma_0=0.6\lambda$, and the wavelength $\lambda=340$ nm corresponds to a plasmon resonance.

around the single cylinder is essentially fully polarized and fully coherent for the beam with $\sigma_0 = 4.8\lambda$. We note that when the coherence length of the incident field is small, the value of the degree of polarization of the near field around the scatterer can significantly differ from unity although the degree of polarization of the incident field is high ($P_3 \approx 0.9$ for $\sigma_0 = 0.6\lambda$ throughout the beam). This is due to the fact that different source points in the scatterer and also the fields that they generate can be weakly correlated for such an incident field. A similar argument can be presented to explain the effects observed in the near-field distribution of the electromagnetic degree of coherence.

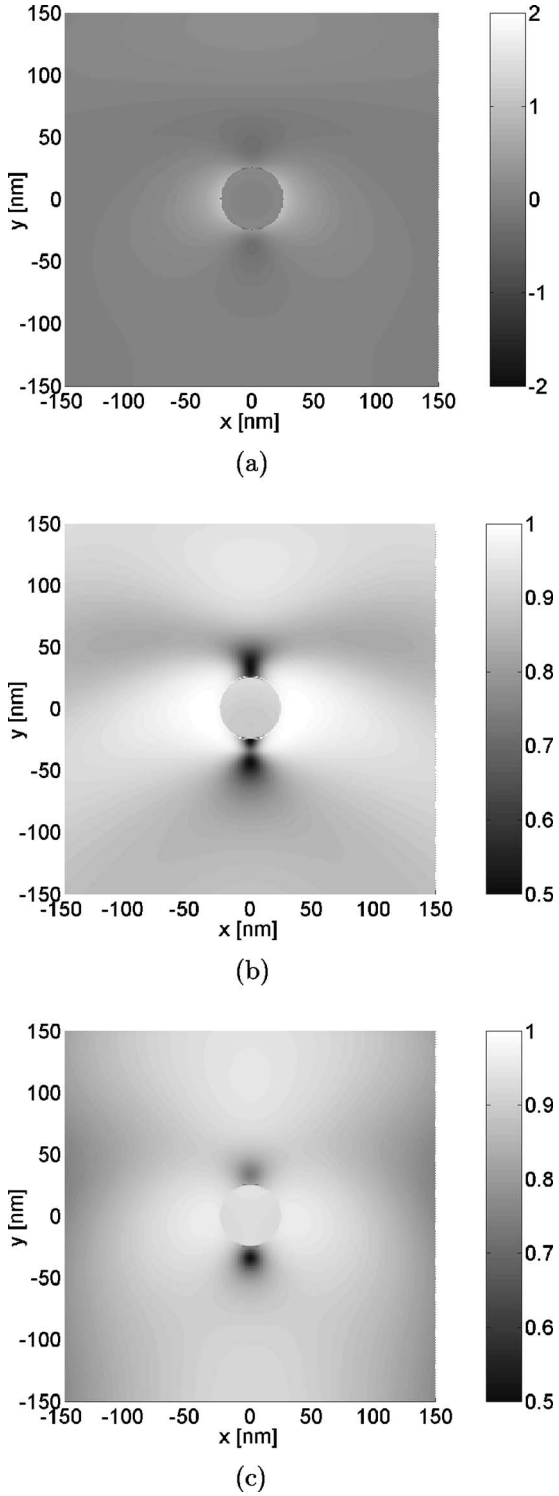

Fig. 2. Same as Fig. 1, except that the wavelength $\lambda = 375$ nm is off resonance.

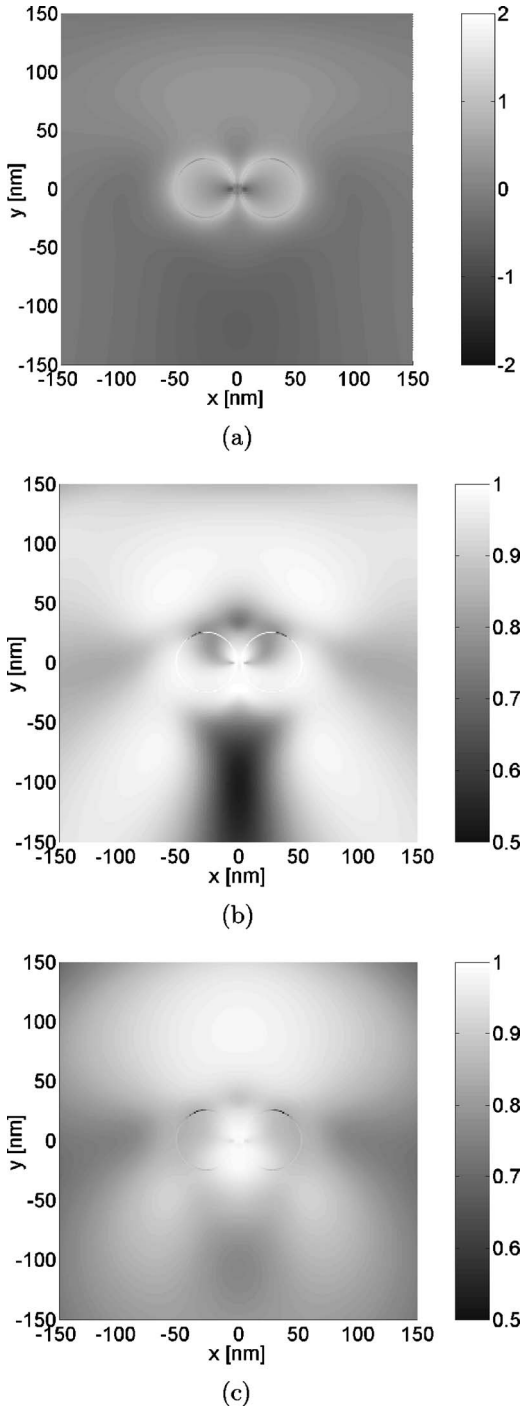

Fig. 3. Illustration of the coherence properties of the near field around two interacting silver cylinders ($r = 25$ nm) with center-to-center separation of 55 nm: (a) spectral density $\log_{10}[S(\mathbf{r},\omega)]$ (arbitrary units), (b) 3D degree of polarization $P_3(\mathbf{r},\omega)$, and (c) electromagnetic degree of coherence $\mu_{el}(\mathbf{r},0,\omega)$. The incident-beam parameters are $w_0 = 4.8\lambda$ and $\sigma_0 = 0.6\lambda$, and the wavelength of light is $\lambda = 340$ nm.

Next we consider a system consisting of two interacting silver cylinders with a center-to-center distance of 55 nm.

From the analysis of the scattering cross section, we know that this two-cylinder system exhibits two resonances: one close to the single-particle resonance peak at $\lambda \approx 340$ nm and another, stronger resonance peak near $\lambda \approx 380$ nm.[5,7,9] Figures 3 and 4 show the results for the wavelengths $\lambda = 340$ nm and $\lambda = 375$ nm, respectively. For $\lambda = 375$ nm the field enhancement is stronger and more localized than for $\lambda = 340$ nm. We also note that for $\lambda = 375$ nm there is a clear similarity in the patterns of the degrees of polarization and coherence to those for the single-particle resonance at $\lambda = 340$ nm [see Figs. 1(b) and 1(c)]. This is in accordance with the fact that the stronger resonance at $\lambda \approx 380$ nm has a more dipolelike character, similar to that of the single-cylinder dipolar resonance, than the weaker resonance at $\lambda = 340$ nm, which is of mixed dipole and quadrupole character.[5]

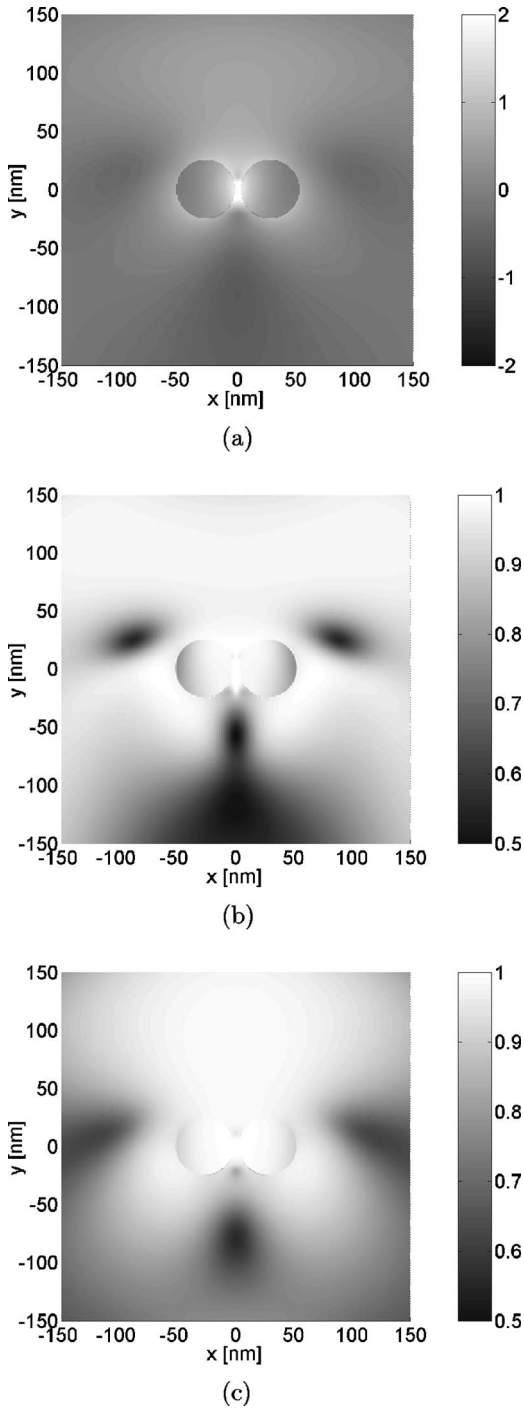

Fig. 4. Same as Fig. 3, except that the wavelength of light is $\lambda = 375$ nm.

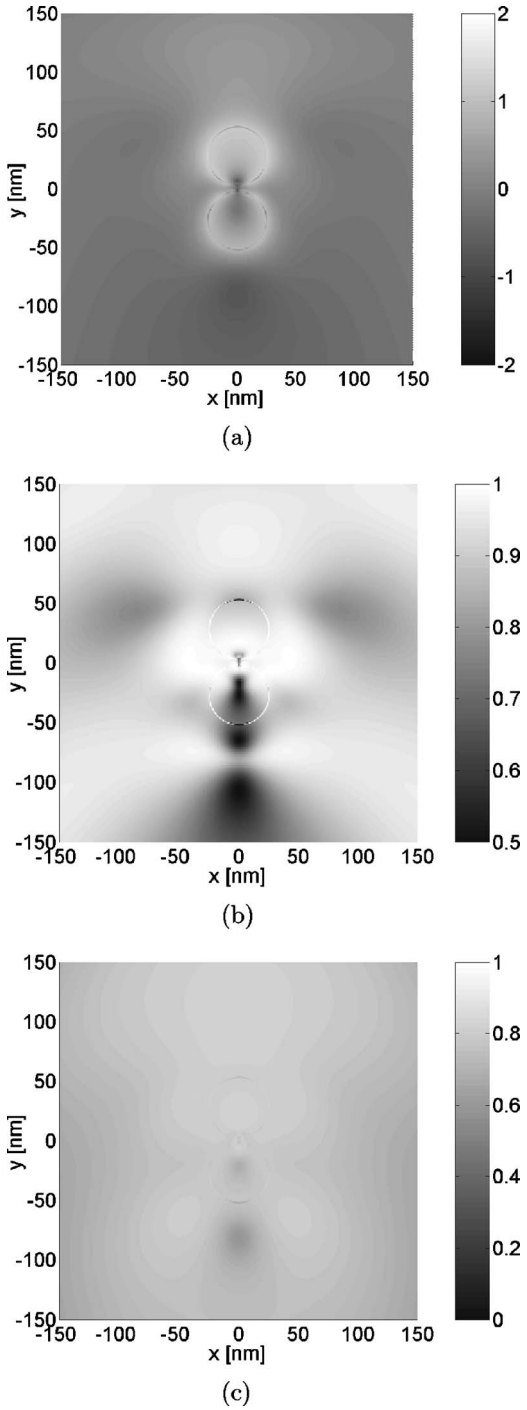

Fig. 5. Same as Fig. 3, except that the cylinder structure has been rotated by 90°.

Figures 5 and 6 depict the quantities $\log_{10}[S(\mathbf{r},\omega)]$, $P_3(\mathbf{r},\omega)$, and $\mu_{el}(\mathbf{r},0,\omega)$ for the wavelengths $\lambda = 340$ nm and $\lambda = 375$ nm, respectively, in the case of two cylinders placed along the symmetry axis of the incident beam with a center-to-center distance of 55 nm. The cylinders exhibit a resonance near $\lambda = 375$ nm for this orientation.[7,9]

Figure 5(a) shows that the enhancement of the intensity mostly takes place close to the boundary of the upper cylinder and that the intensity is quite low in the gap between the cylinders. For $\lambda = 375$ nm we note, instead, that the intensity is strongly enhanced in the gap [Fig. 6(a)]. The electromagnetic degree of coherence with respect to the center point in the gap is shown in Fig. 5(c) for $\lambda = 340$ nm, and we see that the field is quite coherent and that the pattern of $\mu_{el}(\mathbf{r}, 0, \omega)$ is rather smooth. However, for $\lambda = 375$ nm [Fig. 6(c)], we find that the field correlations with respect to the center point of the gap are strong only in the immediate vicinity of the gap and just below the second cylinder.

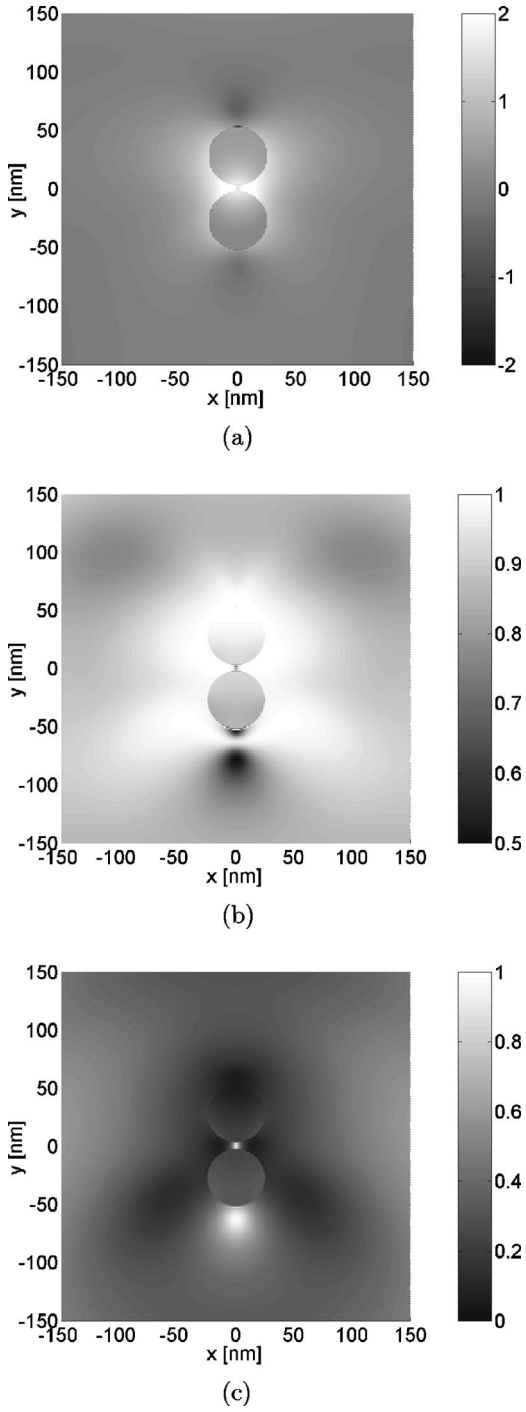

Fig. 6. Same as Fig. 4, except that the cylinder structure has been rotated by 90°.

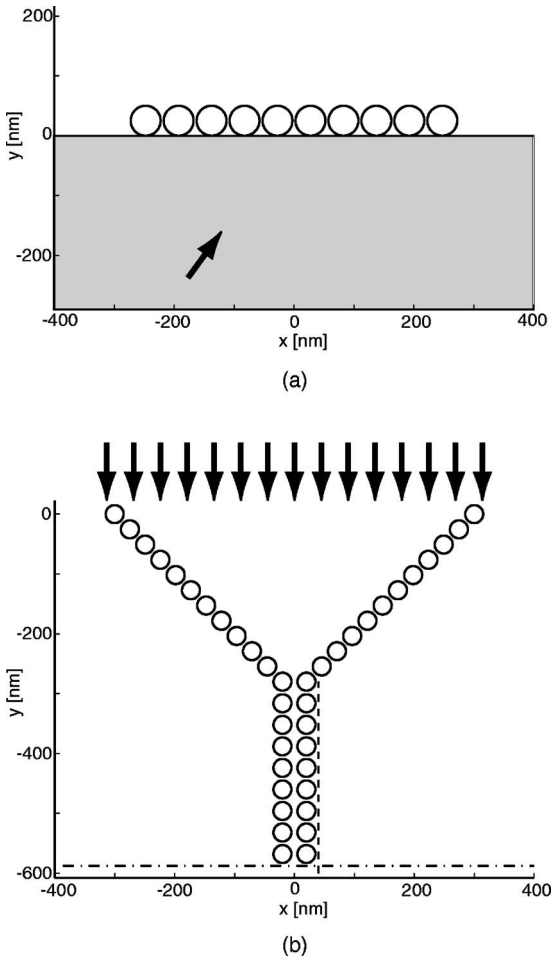

Fig. 7. Illustration of the geometries. (a) Array of ten silver cylinders ($r = 25$ nm) above a glass substrate ($n = 1.5$) with the center-to-center distance of 55 nm. The beam is incident from below, with the propagation direction forming an angle of 54° with respect to the surface normal. (b) Y-shaped structure of silver cylinders ($r = 15$ nm) with the center-to-center distance of 36 nm in the individual chains. The separation of the cylinders between the two vertical chains is 40 nm. The dashed and dashed–dotted lines are explained in the text.

Next we analyze two geometries consisting of several silver nanocylinders. The first system is shown in Fig. 7(a). It consists of ten cylinders of radius 25 nm, with the center-to-center distance between the cylinders being 55 nm. The cylinders are deposited above a glass substrate whose refractive index is $n = 1.5$. The angle of incidence is 54° with respect to the surface normal, so that the cylinders are illuminated by an evanescent wave. Figure 8(a) shows the spectral density along a line 5 nm above the particles for the wavelength $\lambda = 340$ nm for two correlation lengths of the incident beam: $\sigma_0 = 0.6\lambda$ (solid curve) and $\sigma_0 = 4.8\lambda$ (dashed curve). From the figure we observe that the intensity peaks are located above the cylinders and note that the value of the coherence length only slightly affects the intensity distribution above the cylinders at this wavelength. However, the situation is different at the wavelength $\lambda = 412$ nm [see Fig. 8(b)]. In

this case the intensity at the end of the chain is much higher for the beam with shorter correlation length. Furthermore, the intensity peaks are no longer localized above the cylinders but, instead, are seen to lie above the gaps between the cylinders. This feature is similar to that observed for a 3D particle chain above a substrate, which is attributed to an excitation of a collective mode of the chain.[11] Hence our results show that the excitation of such collective chain modes is influenced by the coherence properties of the light.

The Y-shaped configuration of Fig. 7(b) is similar to that analyzed by Gray and Kupka in Ref. 5. The cylinders (r=15 nm) have a center-to-center distance of 36 nm in the individual chains, and the separation of the cylinders between the two vertical chains is 40 nm. The purpose of the structure is to funnel energy from the incident field to the vertex and to locally excite the cylinders of the parallel chains at the vertex. A beam (λ=448 nm and w_0 =4.8λ) is incident on the structure from above. Spectral densities along the double chain are shown in Figs. 9(a) and 9(b) for the beams with correlation lengths of σ_0 =0.6λ and σ_0=4.8λ, respectively. The intensity distributions are seen to be nearly similar in shape. The energy flux in the funnel system is of particular interest in studying the coupling of the incident field into the chain. For this purpose we calculated the Poynting vectors by using Eq. (10). Figure 10(a) shows the normal component of the Poynting vector ($-\langle \mathcal{S}_y \rangle$) along the dotted–dashed line depicted in Fig. 7(b). The plot of the normal component of the Poynting vector, $\langle \mathcal{S}_x \rangle$, at x=40 nm parallel to the double chain, is shown in Fig. 10(b). The results are similar to those presented in Ref. 5, namely, $\langle \mathcal{S}_x \rangle$ along the double chain oscillates in sign [Fig. 10(b)] and has much smaller values than $\langle \mathcal{S}_y \rangle$ at the lower end of the double chain [Fig. 10(a)]. We observe that the behavior of the Poynting vectors is similar for both beams, but the energy flux at the end of the double chain is higher for the spatially more coherent beam.

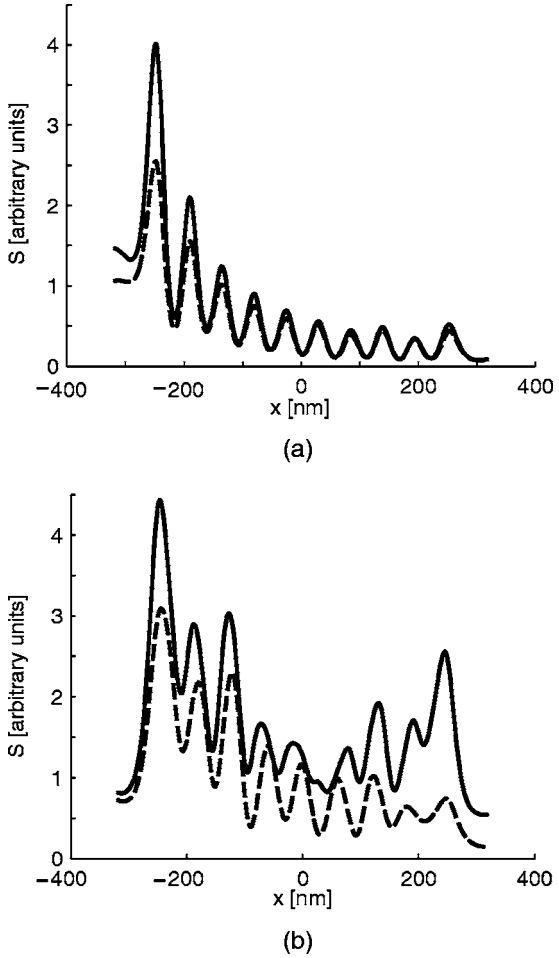

Fig. 8. Spectral density (in arbitrary units) above the nanocylinder chain for wavelengths (a) λ=340 nm and (b) λ=412 nm. The beam parameters are w_0=4.8λ, and σ_0=0.6λ (solid curves) and σ_0=4.8λ (dashed curves).

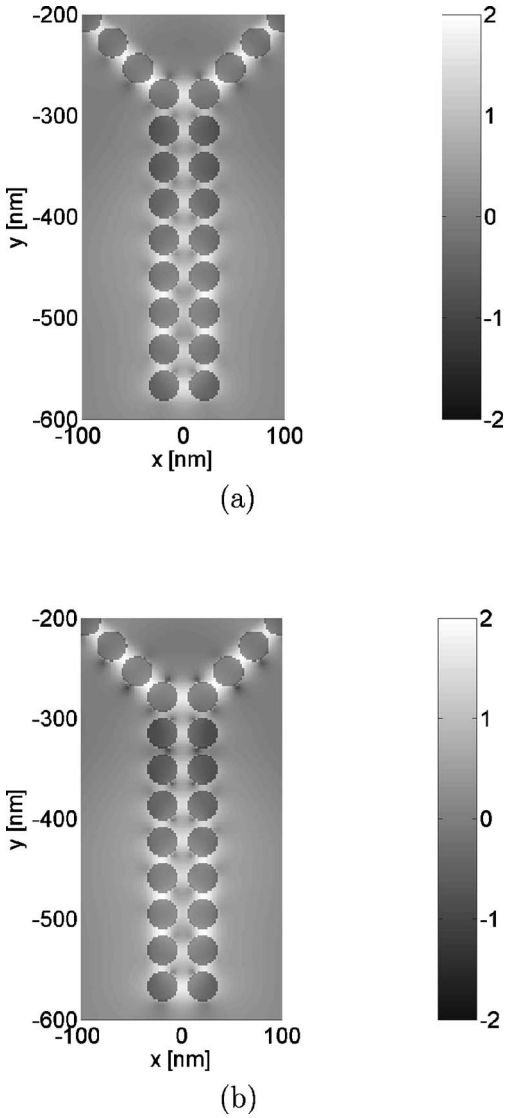

Fig. 9. Spectral density (on $\log_{10}$ scale) around the double chain of the funnel structure. The beam parameters are w_0=4.8λ, and (a) σ_0=0.6λ and (b) σ_0=4.8λ.

7. SUMMARY

In this work we have analyzed the effects of plasmon resonances in metallic nanocylinders on the coherence and polarization properties of the electromagnetic near field

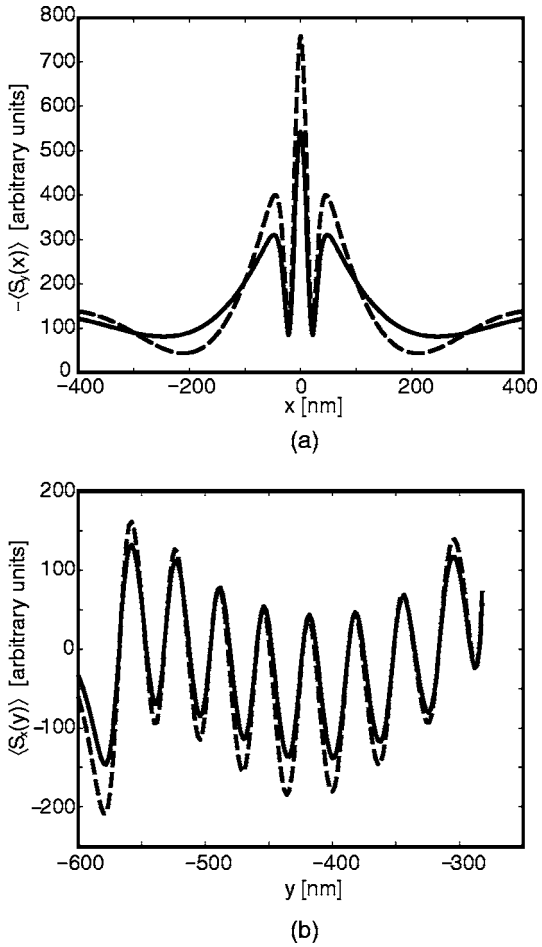

Fig. 10. Illustration of the Poynting vectors in the funnel geometry: normal component of the averaged Poynting vector across the plane (a) 20 nm below the centers of the lowest cylinders in the double chain [dashed–dotted line in Fig. 7(b)] and (b) 20 nm to the right of the centers of the rightmost cylinders in the double chain [dashed line in Fig. 7(b)]. The beam parameters are $w_0 = 4.8\lambda$, and $\sigma_0 = 0.6\lambda$ (solid curves) and $\sigma_0 = 4.8\lambda$ (dashed curves).

when a 1D Gaussian Schell-model TM-polarized beam scatters from the system. We employed the coherent-mode representation of the incident field and solved the scattering problem with the boundary-integral method. Our results show that the plasmon resonances in the cylinders lead to a rich variety of electric field correlation effects in the immediate near zone around the cylinders. We also demonstrated that in nanocylinder chains the partial spatial coherence can influence the coupling of the incident field into the chain and alter the near-field intensity profile.

ACKNOWLEDGMENTS

The authors from Helsinki thank the Academy of Finland for financial support. J. Lindberg acknowledges a grant from the Finnish Cultural Foundation. A. T. Friberg thanks the Swedish Foundation for Strategic Research (SSF) for a senior individual grant.

The corresponding author's e-mail address is Jari.Lindberg@tkk.fi.

REFERENCES AND NOTES

1. R. Carminati and J.-J. Greffet, "Near-field effects in spatial coherence of thermal sources," Phys. Rev. Lett. **82**, 1660–1663 (1999).
2. C. Henkel, K. Joulain, R. Carminati, and J.-J. Greffet, "Spatial coherence of thermal near fields," Opt. Commun. **186**, 57–67 (2000).
3. A. V. Shchegrov, K. Joulain, R. Carminati, and J.-J. Greffet, "Near-field spectral effects due to electromagnetic surface excitations," Phys. Rev. Lett. **85**, 1548–1551 (2000).
4. T. Setälä, M. Kaivola, and A. T. Friberg, "Degree of polarization in near fields of thermal sources: effects of surface waves," Phys. Rev. Lett. **88**, 123902 (2002).
5. S. K. Gray and T. Kupka, "Propagation of light in metallic nanowire arrays: finite-difference time-domain studies of silver cylinders," Phys. Rev. B **68**, 045415 (2003).
6. J. P. Kottmann, O. J. F. Martin, D. R. Smith, and S. Shultz, "Plasmon resonances of silver nanowires with a nonregular cross section," Phys. Rev. B **64**, 235402 (2001).
7. J. P. Kottmann and O. J. F. Martin, "Plasmon resonant coupling in metallic nanowires," Opt. Express **8**, 655–663 (2001).
8. C. Rockstuhl, M. G. Salt, and H. P. Herzig, "Application of the boundary-element method to the interaction of light with single and coupled metallic nanoparticles," J. Opt. Soc. Am. A **20**, 1969–1973 (2003).
9. C. Rockstuhl, M. G. Salt, and H. P. Herzig, "Analyzing the scattering properties of coupled metallic nanoparticles," J. Opt. Soc. Am. A **21**, 1761–1768 (2004).
10. M. Quinten, A. Leitner, J. R. Krenn, and F. R. Aussenegg, "Electromagnetic energy transport via linear chains of silver nanoparticles," Opt. Lett. **23**, 1331–1333 (1998).
11. J. R. Krenn, A. Dereux, J. C. Weeber, E. Bourillot, Y. Lacroute, J. P. Goudonnet, G. Schider, W. Gotschy, A. Leitner, F. R. Aussenegg, and C. Girard, "Squeezing the optical near-field zone by plasmon coupling of metallic nanoparticles," Phys. Rev. Lett. **82**, 2590–2593 (1999).
12. M. L. Brongersma, J. W. Hartman, and H. A. Atwater, "Electromagnetic energy transfer and switching in nanoparticle chain arrays below the diffraction limit," Phys. Rev. B **62**, R16356–R16359 (2000).
13. S. A. Maier, M. L. Brongersma, P. G. Kik, and H. A. Atwater, "Observation of near-field coupling in metal nanoparticle chains using far-field polarization spectroscopy," Phys. Rev. B **65**, 193408 (2002).
14. C. Girard and R. Quidant, "Near-field optical transmittance of metal particle chain waveguides," Opt. Express **12**, 6141–6146 (2004).
15. J.-C. Weeber, A. Dereux, C. Girard, J. R. Krenn, and J.-P. Goudonnet, "Plasmon polaritons of metallic nanowires for controlling submicron propagation of light," Phys. Rev. B **60**, 9061–9068 (1999).
16. G. Schider, J. R. Krenn, W. Gotschy, B. Lamprecht, H. Ditlbacher, A. Leitner, and F. R. Aussenegg, "Optical properties of Ag and Au nanowire gratings," J. Appl. Phys. **90**, 3825–3830 (2001).
17. G. Schider, J. R. Krenn, A. Hohenau, H. Ditlbacher, A. Leitner, F. R. Aussenegg, W. L. Schaich, I. Puscasu, B. Monacelli, and G. Boreman, "Plasmon dispersion relation of Au and Ag nanowires," Phys. Rev. B **68**, 155427 (2003).
18. J. Tervo, T. Setälä, and A. T. Friberg, "Degree of coherence for electromagnetic fields," Opt. Express **11**, 1137–1143 (2003).
19. J. Tervo, T. Setälä, and A. T. Friberg, "Theory of partially coherent electromagnetic fields in the space-frequency domain," J. Opt. Soc. Am. A **21**, 2205–2215 (2004).
20. T. Setälä, A. Shevchenko, M. Kaivola, and A. T. Friberg, "Degree of polarization for optical near fields," Phys. Rev. Lett. **66**, 016615 (2002).
21. L. Mandel and E. Wolf, *Optical Coherence and Quantum Optics* (Cambridge U. Press, 1995).
22. J. Huttunen, A. T. Friberg, and J. Turunen, "Scattering of partially coherent electromagnetic fields by microstructured media," Phys. Rev. E **52**, 3081–3092 (1995).

23. P. A. Knipp and T. L. Reinecke, "Boundary-element method for the calculation of electronic states in semiconductor nanostructures," Phys. Rev. B **54**, 1880–1891 (1996).
24. A. Madrazo and M. Nieto-Vesperinas, "Surface structure and polariton interactions in the scattering of electromagnetic waves from a cylinder in front of a conducting grating: theory for the reflection photon scanning tunneling microscope," J. Opt. Soc. Am. A **13**, 785–795 (1996).
25. J. Wiersig, "Boundary element method for resonances in dielectric microcavities," J. Opt. A, Pure Appl. Opt. **5**, 53–60 (2003).
26. L. Ram-Mohan and L. Ramdas, *Finite Element and Boundary Element Applications in Quantum Mechanics* (Oxford U. Press, 2002).
27. P. B. Johnson and R. W. Christy, "Optical constants of noble metals," Phys. Rev. B **6**, 4370–4379 (1972).
28. It is of interest to note that, unlike in the traditional description of the partial polarization of a plane wave, the electric and magnetic vectors in the present TM-polarized electromagnetic case behave differently. More specifically, since the magnetic field has only a single component H_z, one intuitively would characterize the magnetic field as fully polarized. Indeed, the magnetic cross-spectral density tensor $\mathbf{W}^{(h)}$ at any point $\mathbf{r}$ contains only the element $W_{zz}^{(h)}$, and calculation of the degree of polarization for the magnetic field from Eq. (12), with $\mathbf{W}^{(e)}$ replaced by $\mathbf{W}^{(h)}$, readily gives $P_3^{(h)}=1$. The electric field vector, on the other hand, has both x and y components, and its cross-spectral density tensor at every point is a 2×2 matrix consisting of $W_{xx}^{(e)}$, $W_{xy}^{(e)}$, $W_{yx}^{(e)}$, and $W_{yy}^{(e)}$. For an electric field of this form, it has been shown[20] that the 3D degree of polarization takes on values $1/2\leqslant P_3^{(e)}\leqslant 1$.